Energy Reports 6 (2020) 3230–3239

Contents lists available at ScienceDirect

Energy Reports

journal homepage: www.elsevier.com/locate/egyr

Pyrolysis characteristics and kinetics of human faeces, simulant faeces and wood biomass by thermogravimetry–gas chromatography–mass spectrometry methods

Tosin Somorin [a,*], Alison Parker [b], Ewan McAdam [b], Leon Williams [b], Sean Tyrrel [b], Athanasios Kolios [a], Ying Jiang [b]

[a] University of Strathclyde, Glasgow, G1 1XQ, UK
[b] Cranfield, University, MK43 0AL, UK

ARTICLE INFO

Article history:
Received 29 April 2020
Received in revised form 12 October 2020
Accepted 15 November 2020
Available online 9 December 2020

Keywords:
Hyphenated techniques
Non-isothermal conditions
Faecal sludge
Evolved gas analysis
Onsite sanitation

ABSTRACT

Human faeces (HF) are treated as wastes in many parts of the world, a resource that can be converted to energy and fuels. To enhance the understanding of fuel conversion processes and decomposition characteristics, this study investigated the pyrolysis behaviour and evolved gas profiles of HF using thermogravimetry with gas chromatography–mass spectrometry methods. Kinetic parameters were deduced using model-free kinetic models. Results are compared with simulant faeces (SF), wood biomass (WB) and HF–WB blends. The pyrolysis of HF involved two decomposition peaks — a fronting peak with weight loss of ∼51 wt% and a tailing shoulder peak with weight loss of ∼15 wt%. The apparent activation energy for HF varied from 122–382 kJ/mol at conversion rates of 10%–90% using Kissinger–Akahira–Sunose model. Some of the key pyrolysis products for HF at 370 °C were 4-methoxy-phenol, n-hexadecanoic acid, phenol, 4-methyl- and indole isomer (pyrrolo[1,2-a]pyridine). At 530 °C, evolved gases were largely fragmented with high proportions of alkanes and alkenes including 3-dodecane, 2-undecane, 6-tridecene, 2-propenylidene-cyclobutene. These products differed to WB that are largely hydroxyphenyls and methoxyphenols with guaiacyl or syringil structures. Blending with WB improved pyrolysis of HF, irrespective of the proportions of blend.

© 2020 The Authors. Published by Elsevier Ltd. This is an open access article under the CC BY-NC-ND license (http://creativecommons.org/licenses/by-nc-nd/4.0/).

1. Introduction

The need to transit to a sustainable future is changing the way we manage natural resources and waste. Organic materials (e.g. food wastes, crop residues and manure) that are usually treated as waste, are nowadays considered valuable feedstocks for chemicals, fuels and energy (Lens et al., 2004; He et al., 2008). This includes human excreta (urine and faeces), resources that would otherwise be sent to the wastewater treatment plant and in many parts of the world, inappropriately disposed into the environment (Strande and Brdjanovic, 2014; Diener et al., 2014). These materials are now increasingly explored for: (a) agriculture e.g. as a soil conditioner (Yadav et al., 2010; Bai et al., 2018), (ii) production of animal protein (Nyakeri et al., 2017), (iii) recovery of macro- and micro-nutrients (Mihelcic et al., 2011), (iv) building materials (Diener et al., 2014) and (v) heat and electricity (Ieropoulos et al., 2012; Onabanjo et al., 2016a).

The use of human faeces for energy generation is gaining reputation because faeces are a rich biomass source: consisting of undigested fats, protein, polysaccharide, bacterial biomass, unabsorbed nutrients, gut secretions, digestive juices and cell shedding (Rose et al., 2015). They can be subjected to heat, like any biomass material, with or without the presence of oxygen to generate valuable energy products including faecal char and solid fuel. Previous work by the authors has shown that there is the prospect for energy and water recovery through efficient combustion of faeces and membrane purification of urine (Hanak et al., 2016; Kolios et al., 2018). However, efficient conversion requires a good understanding of the decomposition characteristics, particularly devolatilization processes.

Devolatilization (or pyrolysis) provides the advantages of moderate temperatures (350–500 °C) and oxygen-depleted environment, which potentially can reduce emissions and energy consumption in solid fuel conversion (Kumar et al., 2017). It is an important step in thermochemical conversion that can be combined with other advanced thermal processes such as gasification and combustion, to reduce waste volume and improve process efficiency (Basu, 2010; Gvero et al., 2016). The process follows drying and can proceed into gasification and/or combustion if oxidant is present in limited and/or sufficient quantities. Depending on the feedstock, process conditions and technology

* Corresponding author.
E-mail address: tosin.somorin@strath.ac.uk (T. Somorin).

https://doi.org/10.1016/j.egyr.2020.11.164
2352-4847/© 2020 The Authors. Published by Elsevier Ltd. This is an open access article under the CC BY-NC-ND license (http://creativecommons.org/licenses/by-nc-nd/4.0/).

used, multiple end products (char, gas, bio-oil) can be derived (Chun et al., 2011; Danso-Boateng et al., 2013) e.g. as a solid fuel in furnaces and kilns or for soil amendment (Herzen and Talsma, 2014). Resource recovery will depend on the amount, quality and composition of products, which in turn depend on complex heterogeneous solid-state reactions, processes that are poorly understood for human faeces.

Thermogravimetric analysis (TGA) provides key information on reaction stages as it quantifies the change in mass of a material with respect to time or temperature as materials are subjected to controlled heating conditions (Pasangulapati et al., 2012; Slopiecka et al., 2012). In combination with other analytical devices, the thermo-mechanical, -physical and -chemical properties of materials can be determined. For instance, the coupling of TGA with Fourier-Transform Infrared Spectroscopy (FTIR) and/or Gas Chromatography–Mass Spectrometry (GC–MS) allows the qualification and/or quantification of evolved gases (Wu et al., 2009; Magdziarz and Werle, 2014; Wang et al., 2010). These hyphenation techniques have proven to be useful for material characterization for sewage sludge (Singh et al., 2012; Lin et al., 2016), animal manure (Rodríguez-Abalde et al., 2013) and other organic wastes (Özsin and Pütün, 2017) but limited work has been completed for human faeces.

A few studies that have investigated the thermochemical conversion of human faeces have focused on the development of energy conversion systems and operating conditions (Onabanjo et al., 2016a; Ward et al., 2014; Jurado et al., 2018; Gold et al., 2018) with limited understanding of fuel conversion processes and interaction. From studies completed, there is the understanding that temperature and residence time are factors affecting the yield and quality of products (Ward et al., 2014; Liu et al., 2014; Gold et al., 2018). Operating temperature of 300 °C is suggested to be suitable for fuel production but those above 600 °C were not recommended for faecal char. The carbon stability of faecal char at 450–600 °C was found to be similar to those obtained from lignocellulose biomass, though significantly lower in proportion. Faecal char and briquette production can be achieved but beyond these, there is paucity of information on decomposition behaviour and kinetics. Studies by Yacob et al. (2018) that reported some information on decomposition products of HF have focused on selected gas products (CO, CO_2, CH_4, C_2H_6, H_2), and previous work by the authors (Fidalgo et al., 2019) have not considered evolved gases.

Thus, this paper presents the pyrolysis behaviour and evolved gas profiles of HF using TG–GC–MS. Results are compared with those obtained from wood biomass (WB) and HF–WB blends to identify reactivity change and potential synergistic effects between materials. simulant faeces are examined to ascertain their suitability as an alternative in the analysis of HF. Kinetic parameters i.e. activation energy and pre-exponential factor, associated with these processes are determined using non-isothermal model-free methods. The influence of operating conditions was examined at various heating rates (5–100 K/min) and fuel blending conditions. Knowledge arising from this study can enhance the understanding of the reaction mechanisms underlying the pyrolysis of HF and the importance of fuel blending in fuel conversion and reaction rates. It can inform the design of an appropriate energy system for optimum yield of products. Insights on evolved gas streams can inform strategies on emission reduction and abatement options, processes that can undermine the prospect of energy recovery if not well understood.

2. Materials & methods

2.1. Sample preparation and characterization

Fresh human faeces were collected anonymously from volunteers, as part of the Nano-membrane Toilet Project "Sample Collection Campaign" and under the approval of the Institution's Research Ethics Committee (CURES/2310/2017). All samples were stored at −85 °C during the collection period to preserve material, then subsequently brought to room temperature, mixed and dried at 105 °C to constant weight. Simulant faeces (SF) was prepared using the "Recipe 9" listed in Onabanjo et al. (2016b). Wood biomass (WB) was sourced from Cranfield energy laboratory facilities and hardwood derived product although exact source not indicated. Blended samples were prepared at HF to WB ratios of 20:80 (HF20), 40:60 (HF40), 60:40 (HF60) and 80:20 (HF80), then dried at 105 °C to constant weight. All samples including wood biomass (WB) were manually grounded into particle sizes of <2 mm. The elemental composition of the samples was determined using Elementar Vario ELIII CHN Elemental Analyser. This involved the determination of the relative percentages of carbon (C), hydrogen (H) and nitrogen (N) as outlined in BS EN ISO 16948. The wt.% of C, H, N and ash were deducted from 100% to determine oxygen (O) content. The relative percentages of moisture, volatile matter and ash were determined using thermogravimetric methods (Saldarriaga et al., 2015) and fixed carbon as a balance. The Higher Heating Values (HHVs) were deduced from the correlation in Eq. (1) (see Table 1).

$$\mathrm{HHV\ (MJ/kg)} = 0.3491\,(\mathrm{C}) + 1.1783\,(\mathrm{H}) - 0.1340\,(\mathrm{O}) - 0.151(\mathrm{N}) - 0.0211\,(\mathrm{Ash}) \quad (1)$$

2.2. Thermogravimetric analysis

A thermogravimetric analyser (Perkin-Elmer TGA 8000, Llantrisant, UK) was used to investigate the thermal decomposition behaviour of HF and blended samples. 18 ± 1 mg of dried HF, WB and SF and HF–WB blends (HF20-80) were subjected to non-isothermal heating in the thermogravimetric analyser. Each sample was placed in an aluminium crucible under high-purity nitrogen (99.999%) at a gas flow rate of 45 mL/min. For all samples, the temperature was raised from 105 to 850 °C at 5, 25, 50, 75 and 100 °C/min for HF and 50, 75 and 100 °C/min for other samples and blends to reduce analysis time. Prior to the ramp temperature regime, samples were held for at least 5 min at 105 °C and thereafter at 850 °C. For repeatability, each test was conducted in triplicates and the average reported.

2.3. Evolved gas analysis

The evolved gas was sampled from the TGA at target temperatures of 370 °C and 530 °C for HF, 350 and 435 °C for WB and, 330 and 475 °C for SF, corresponding to the stages of highest devolatilization. 1 ml of the sample gas was obtained at an injection time of 10 s and the rest was automatically purged out of the system. The sampled gas was then transferred to a single quadrupole GC/MS (PerkinElmer Clarus® SQ 8, Llantrisant, UK) equipped with a fused silica capillary column (Extile, 60 m × 0.25 mm × 0.25 μm film thickness) The transfer of gas was achieved via an automated transfer line that is maintained at 270 °C to prevent condensation. The TGA temperature was set to rise from 105–850 °C under nitrogen atmosphere a heating rate of 100 °C/min, carrier gas flow rate of 45 mL/min, with isothermal heating at 105 and 600 °C for 5 min before and after non-isothermal heating regime respectively. The GC oven temperature was set at the following conditions: hold temperature of 50 °C for 1 min, followed by ramp temperature from 50–250 °C 10 °C/min and then a final hold temperature of 250 °C for 10 min. High-purity helium was used as a carrier gas for the column at a gas flow rate of 1 mL/min. The source temperature for the MS was set at 280 °C. The unit was operated in electron impact ionization

Table 1
Proximate, Ultimate and lower heating values of the biomass samples.

Samples	Proximate analysis (wt.% db)			Ultimate analysis (wt.% db)				Estimated HHV (MJ/kg)
	Volatile matter	Ash content	Fixed carbon	C	H	N	O	
HF	74.80	14.80	10.39	49.41	7.62	5.31	22.86	22.05
SF	75.71	24.25	0.04	44.85	7.24	2.52	21.14	20.46
WB	82.71	1.43	15.86	48.96	6.88	0.08	42.65	19.44

mode at ionizing energy of 70 eV with full scan mass detection (scan rate of 0.02 s and 30–450 m/z).

The identification of all the chemical species was attempted by comparing the mass spectral of each of the peaks in the chromatogram with templates in NIST databases. For data quality, chemical species with reverse match factor of >850 were only considered. Across all feedstocks, low molecular weight, highly volatile compounds and hydrocarbons such as propanol, urea, ethylene oxide, ethyne fluoro, methyl nitrite, carbamic acid, methanethiol and cyclopropyl carbinol, eluted almost together at a residence time of 2.05–2.18 s, along with non-condensable gases e.g. CO_2 and N_2O. These compounds are difficult to differentiate, particularly for elements with similar molecular weight e.g. N_2 and CO, because at the low end of the scanning range, m/z ratio of <40, low molecular weight compounds, hydrocarbons and non-condensable gases contribute to background signals when present.

2.4. Kinetic analysis

The rate equation that defines the isothermal decomposition of solid fuels is shown in Eq. (2).

$$\frac{\partial\alpha}{\partial t} = kf(\alpha) \tag{2}$$

where, k is the temperature-dependent rate constant, f(α) is the function of α. The degree of conversion, α has linear relationship with k and can be defined using Eq. (3).

$$\alpha = \frac{m_i - m}{m_i - m_f} \tag{3}$$

m_i and m_f are initial and final weight while m is the actual sample weight at a given time (t).

$$k = A\ \exp\left(-\frac{E_a}{RT}\right) \tag{4}$$

$$\frac{\partial\alpha}{\partial t} = A\exp\left(-\frac{E_a}{RT}\right) f(\alpha) \tag{5}$$

Using the Arrhenius expression for sample decomposition in Eq. (4), the rate equation is transformed into Eq. (5), which describes the degree of conversion of the sample with time. Here, A is pre-exponential or frequency factor (1/min), T is the absolute temperature in K, and R is the universal gas constant (8.314 J/mol K) and E_a is activation energy (kJ/mol). However, under non-isothermal conditions with constant (linear) heating rate, $\beta = \frac{\partial T}{\partial t}$, the rate equation assumes the expression in Eq. (6). Here, kinetic parameters (apparent activation energy and pre-exponential factor) are determined using various modelling approaches and analytical techniques, including differentiation, integration and approximation methods.

$$\frac{\partial\alpha}{\partial t} = \frac{A}{\beta}\exp\left(-\frac{E_a}{RT}\right) f(\alpha) \tag{6}$$

In this study, model-free iso-conversional methods including as Friedman (FD) and Kissinger–Akahira–Sunose (KAS) are explored. Both methods assume that the degree of conversion is constant, and the rate constant depends on temperature. FD method further assumes that the conversion term f(α) is constant, hence the thermal decomposition processes depend on the mass-loss rate rather than on temperature.

The integration of Eq. (6) gives Eq. (7).

$$g(\alpha) = \frac{\partial\alpha}{\partial t} = \frac{A}{\beta}\int_0^T \exp\left(-\frac{E_a}{RT}\right)\partial t \tag{7}$$

Here, the activation energy is obtained from the slope of ln $\left(\frac{\partial\beta}{\partial t}\right)$ versus 1/T and the pre-exponential factor is obtained from the intercept.

$$\ln\frac{\partial\alpha}{\partial t} = \ln\left[\beta\left(\frac{\partial\alpha}{\partial t}\right)\right] = \ln[(f(\alpha))] - \frac{E_a}{RT} \tag{8}$$

KAS method (Eq. (8)) assumes that the conversion term, α have a constant value and adopts the approximation in Eq. (9) for $20 \le x \le 50$ to obtain Eq. (10).

$$\log p(x) = \frac{\exp^{-x}}{x^2} \tag{9}$$

$$\ln\frac{\beta}{T_m^2} = -\frac{E_a}{RT}\left(\frac{1}{T_m}\right) - ln\left[\left(\frac{E_a}{AR}\right)\int_0^\alpha \frac{\partial\alpha}{f(\alpha)}\right] \tag{10}$$

where T_m is the temperature at the maximum reaction rate. The activation energy is then obtained from the slope of the plot of ln $\left(\frac{\beta}{T_m^2}\right)$ versus 1/ T_m (K) and the pre-exponential factor is from the intercept. In both cases, apparent activation energy and pre-exponential factor were determined for the degree of conversion intervals of $0.10 < \alpha < 0.90$.

3. Results & discussion

3.1. Pyrolysis characteristics

The thermogravimetric (TG) and derivative thermogravimetric (DTG) curves for the pyrolysis of HF at 50 °C/min under N_2 atmosphere are shown in Fig. 1. The results show that there are two decomposition peaks and three thermal stages for the pyrolysis of HF100. A slight weight loss (∼5%) is observed at temperatures <185 °C (1st stage), which cannot be attributed to moisture removal, as often reported in other studies (Saldarriaga et al., 2015). This is because samples had been dried at 105 °C prior to analysis. A major decomposition peak is observed at about 355 °C and within temperature ranges of 185–450 °C (2nd stage). Following this, a shoulder peak is observed at about 488 °C in the 3rd thermal stage, temperatures of 450–600 °C. The weight loss for the major decomposition stages are 51 wt% (2nd stage) and 15 wt% (3rd stage). These correspond to weight loss rates of 3.09 mg/min and 0.84 mg/min respectively. The overall weight loss leaves the residual weight of the char at about 30 wt%.

Studies by Liu et al. (2014), Ward et al. (2014) and Gold et al. (2018) have showed that pyrolysis temperature of 300 °C can affect the quality of faecal char as fuel, due to progressive loss of energy-rich hydrocarbons and an increasing amount of ash. Unlike coal fuels, where low pyrolysis temperature improves HHVs via decarboxylation, aromatization, condensation and polymerization, low heat can cause thermal degradation of biomass feedstocks. This study shows that HF has considerably low onset

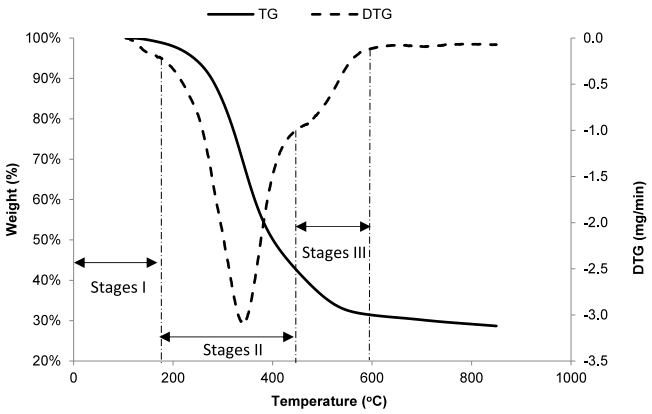

Fig. 1. TG & DTG curve of HF in N_2 atmosphere and at 50 °C/min.

temperature with slight weight loss observed at temperatures <200 °C, possibly due to the release of highly volatile compounds and hydrocarbons. These findings have implications on design considerations for faecal sludge drying if downstream energy recovery is an option. To avoid thermal decomposition, it will be important to keep drying temperatures at a minimum, that is the heat supplied should be enough to drive the endothermic processes for drying but insufficient to initiate devolatilization. The thermal stages and temperature ranges suggest the optimum conditions for thermochemical conversion of HF. They provide insights on thermal stability and multi-step decomposition behaviour of HF feedstocks. The influence of heating rate, fuel variation and blending is considered in Sections 3.1.1–3.1.3.

3.1.1. Influence of heating rate

The TG and DTG curves from the pyrolysis of HF at various heating rates of 5–100 °C/min are illustrated in Fig. 2, which indicate the influence of heating rate on weight loss behaviour. The maximum weight loss rate increased with increasing heating rates: 0.30, 1.54, 3.09, 4.50 and 5.6 mg/min at 5, 25, 50, 75 and 100 °C/min respectively. The maximum temperatures for devolatilization also increased with increasing heating rates: corresponding to 316, 344, 355, 376 and 392 °C at 5–100 °C/min. The onset and burn-out temperatures were similar in all cases, although slightly extended at higher rates. The increase in maximum weight loss rate can be attributed to a rapid fragmentation of the feedstock while increasing maximum temperature is caused by heat and mass transfer limitations that occur at higher heating rates. Here, thermal events are overtaken by a rapid rate of increase in temperature (Fidalgo et al., 2019). For all the heat rate conditions, the final weight of the residues was relatively the same.

The maximum weight loss reported in this study are higher than the <0.04 mg/min obtained in Yacob et al. (2018) at heating rates of 1–10 °C/min. The DTG curves also differed slightly: minor peaks are observed at 271–292 °C, major peaks at ∼309–332 °C and tailing shoulder peaks at <400 °C for the various heating rates. These suggest variations in the chemical composition of the feedstocks. Rose et al. (2015) have shown that the chemical composition of HF can vary significantly, depending on dietary intake, fibre content, body weight and age. To identify, predict and model the influence of fuel variation, reliable kinetic estimates are required. These can be obtained using the decomposition curves in Fig. 2 at various heating rates.

3.1.2. Comparison with various biomass feedstocks

The TG and DTG curves for the pyrolysis of HF and in comparison, to SF and WB at 50 °C/min are shown in Fig. 3. The overall weight loss for the feedstocks is 76 wt% (WB) and 67 wt. % (SF and HF) —Fig. 3a. The DTG pattern for the HF is dissimilar to those obtained from SF and WB, which suggest that the decomposition characteristics for these samples are different (Fig. 3b). For the SF, there are three distinct peaks: the first maximum decomposition peak is observed at 315 °C, the next at 359 °C and the last at about 455 °C. For the WB, there is a prominent decomposition peak with a maximum temperature at 415 °C but a fronting shoulder peak between 290–350 °C. The maximum weight loss rate was 5.86 mg/min for the WB while the values for SF100 and HF100 were 2.90 and 3.09 g/min respectively, at the same heating rate. The burn-out temperature for WB was significantly lower than other fuels at 466 °C, although the onset temperature was similar to other feedstocks. As observed in Fig. 3, HF was more reactive to low heat than other fuels, and SF showed a similar tendency. This was however different for WB, as a flat curve is observed before its onset temperature.

The various peaks in the DTG curves (Fig. 3b) correspond to the decomposition of various complex organic compounds. According to Kim et al. (2006), Poletto et al. (2012) and Zhang et al. (2018), the decomposition of hemicellulose, cellulose and lignin, the major components in wood, occur at about 180–350 °C, 275–350 °C and 250–500 °C respectively. These components behave differently under heat due to their chemical composition (Chen and Kuo, 2011). Cellulose is a crystalline polysaccharide with a linear, non-branching chain of 1-4-β-D- glucopyranose that gives wood its characteristic thermal stability. Hemicellulose has a random amorphous structure with short, highly branched molecular chains that easily get hydrolysed (Wang et al., 2017). Lignin is a heavily cross-linked phenolic polymer with high aromatic rings that are highly stable and difficult to decompose. As such, in the presence of heat, these compounds progressively fragment with the highly extractive components, i.e. low molecular mass and volatile compounds, aiding ignition and thermal degradation of other compounds. The result in Fig. 3 shows that the decomposition characteristics of WB differ to HF.

A study by Zhou et al. (2018) has shown that beef and dairy cattle manure exhibit four pyrolysis stages and temperature ranges differed from those reported in this study. For sewage sludge, a major decomposition stage is typically reported between 150–600 °C (Nowicki and Ledakowicz, 2014) and in some cases with series of tailing peaks (Naqvi et al., 2018), indicating complex heterogeneous solid-state reactions. Decomposition is also observed at temperatures above 650 °C, which is attributed to the thermal degradation of low-temperature thermal-stable components. For example, Wang et al. (2016) reported two overlapping decomposition peaks at 200–550 °C and a single peak at 600–750 °C. This differing multi-step decomposition behaviour to HF suggest that faecal related materials such as sewage sludge and animal manure, are not necessarily model materials for HF. Also, SF has been frequently used in a number of studies for modelling HF (Penn et al., 2018; Radford et al., 2015; Jurado et al., 2018); however, this study shows that SF has different decomposition behaviour to HF and do not accurately model the pyrolysis process.

3.1.3. Influence of fuel blending

The TG and DTG curves for the HF–WB blends are shown in Fig. 4, indicating the effects that blending can have on thermal decomposition behaviour of faecal biomass.

The DTG curves in Fig. 4b shows that blending of WB with HF improved the decomposition of the HF, irrespective of the proportions of the blend. All the HF–WB blends had a similar

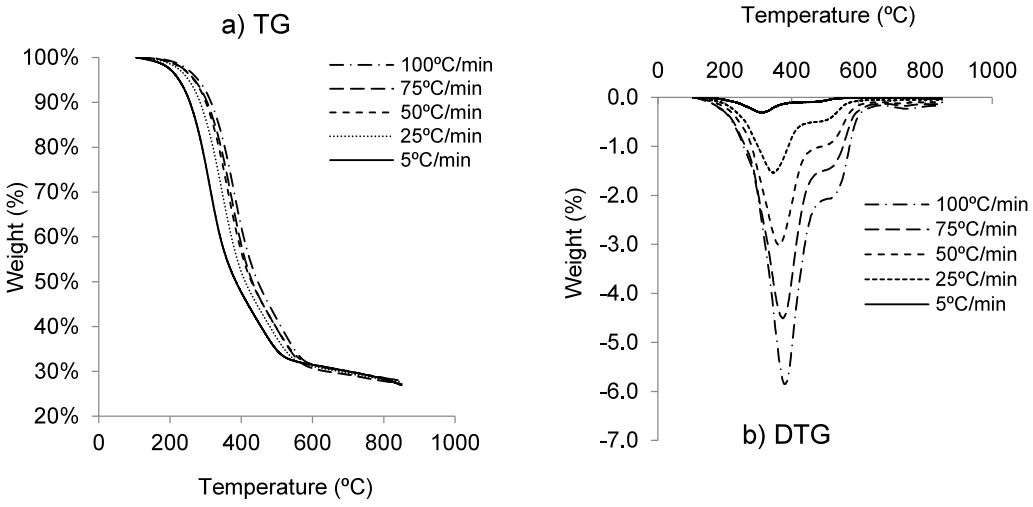

Fig. 2. TG & DTG curves of HF in N_2 atmosphere at various heating rates (5–100 °C/min).

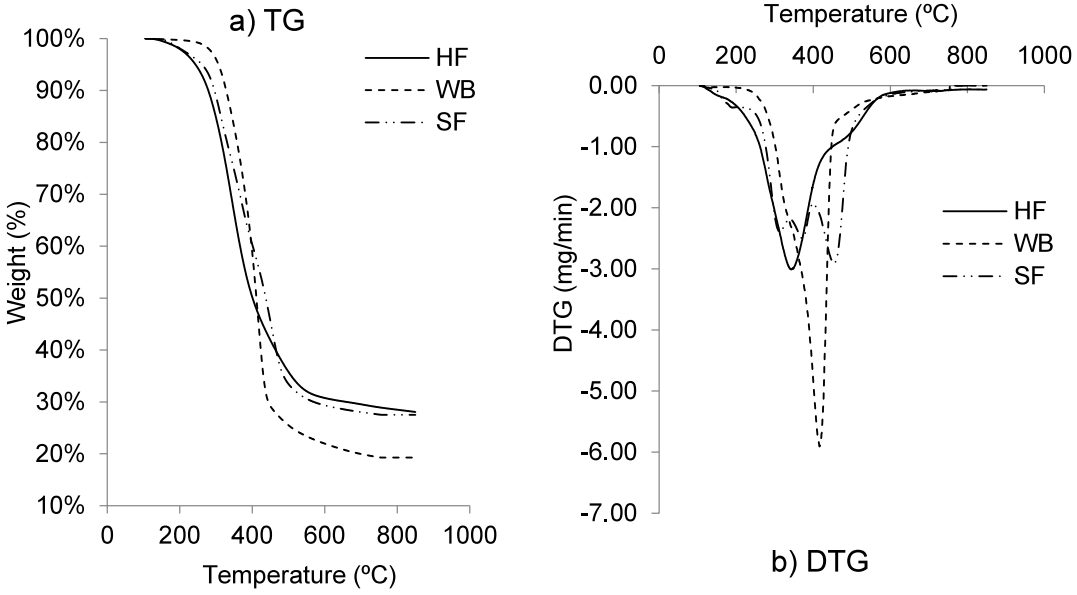

Fig. 3. TG & DTG curves of HF, WB & SF at 50 °C/min (N_2).

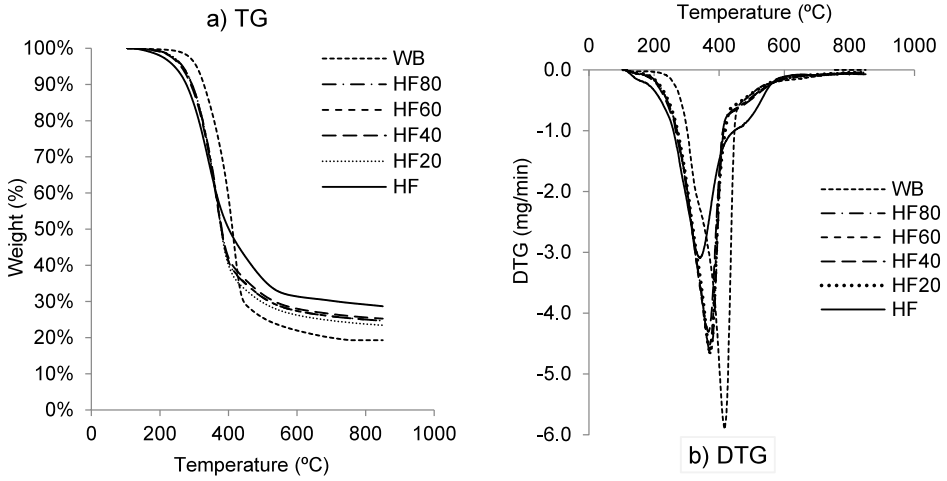

Fig. 4. TG & DTG curves of HF–WB blends at 50 °C/min (N_2).

Table 2
Kinetic data (Ea, A and R^2) for HF decomposition for Friedman and KAS models.

α	Friedman (FD)			Kissinger–Akahira–Sunose (KAS)		
	Ea (kJ/mol)	lnA (min^{-1})	R^2	Ea (kJ/mol)	lnA (min^{-1})	R^2
0.1	124.56	24.74	0.996	121.56	17.68	0.998
0.2	141.15	27.19	0.995	130.78	17.86	0.998
0.3	139.41	25.95	0.997	135.85	17.56	0.998
0.4	138.71	25.03	0.973	142.24	18.13	0.999
0.5	159.10	28.13	0.997	147.07	18.18	0.998
0.6	186.34	31.86	0.986	169.88	21.40	0.997
0.7	229.94	37.38	0.979	220.63	28.72	0.986
0.8	278.61	42.39	0.982	282.36	36.10	0.986
0.9	413.34	59.29	0.982	382.35	47.78	0.979
Avg.	**201.24**	**33.54**	**0.987**	**192.52**	**24.82**	**0.993**

decomposition pattern as the parent material, HF until pyrolysis temperature of 378 °C was reached. Above this temperature, the peak intensity of the decomposition curves for the HF–WB blends increased significantly by more than 50%. The tailing shoulder peak for the HF–WB blends is observed to be reduced to HF100 counterpart, indicating further decomposition had occurred. This study shows that blending ratio had minimal effect on the maximum weight loss rate, as peak intensities for all the blends were similar, and between those of their parent material. These results suggest synergy between WB and HF, particularly at high temperatures. Similar observations are reported in Yuan et al. (2012), Krerkkaiwan et al. (2013), Farrow et al. (2013) and Li et al. (2014), with attribution to synergistic interactions between pyrolytic products at high temperatures. Here, char catalytic effects, radical interactions and secondary interactions are suggested to promote synergistic interactions. Wang et al. (2016) showed that the co-pyrolysis of sewage sludge and microalgae biomass altered the decomposition behaviour of the sewage sludge, which was accounted to random nucleation and growth reaction mechanisms at temperatures above 550 °C. Other authors (Moghtaderi et al., 2004; Gil et al., 2010; Aboyade et al., 2013; Lu et al., 2013) accounted synergistic interactions to additive behaviour, where blends behave independently and does not interact with other components. This study cannot ascertain the factors promoting suggested synergistic interactions; however, the results show that blending HF with WB improved weight loss rate by 91%, as such HF can be blended with other biomass materials for energy generation. Previous work by the authors (Somorin et al., 2017) has shown that 50:50 WB: HF blend reduced moisture levels by 40% prior to drying and improved conversion.

3.2. Reaction kinetics

The apparent activation energy (Ea) and pre-exponential factor (A) that define reaction kinetics are listed in Table 2, along with their measure of fitness and, as obtained from FD and KAS models at conversion rates (α) of 10%–90%. The results show that Ea increases with the degree of conversion, as similarly observed in Chen et al. (2014) for the pyrolysis of Moso bamboo. At conversion rates of 40% and more, Ea increased from approximately 139–413 kJ/mol and 142–382 kJ/mol using FD and KAS models respectively. The KAS method had the best measure of fitness (avg. $R^2 = 0.993$); hence, the most suitable model for defining the pyrolysis of HF. Here, the average Ea and A are 192.52 kJ/mol and 24.82 s^{-1} respectively.

The Ea values reported in this study are lower than the 241.5 ± 2.9 kJ/mol in Yacob et al. (2018) but significantly higher than those reported in the literature for other feedstocks. Studies by Lu et al. (2013) have shown that the average Ea in coal and wood are about 74 and 77 kJ/mol respectively. Related materials such as sewage sludge are reported with average E_a values of 23.6–76.4 kJ/mol (Xu et al., 2018; Zhai et al., 2011; Naqvi et al., 2019). Cotton stalks (CS) and sugarcane bagasse (SB) are reported to have Ea values varying from 98.5–100.2 kJ/mol (CS) and 43.0–53.5 kJ/mol (SB) when direct Arrhenius plot and integral methods were used, and 72.5–127.8 kJ/mol (CS) and 77–87.7 kJ/mol (SB) when obtained from integral methods (El Sayed and Mostafa, 2015). The relatively high Ea observed in this study suggest that complex large molecules are present in HF, especially at the later stages of conversion (>50%). This would be expected because HFs are compounded mixtures of undigested and unabsorbed foods locked in a bulky matrix of bacterial biomass. These materials have undergone mechanical, biological and chemical digestion, processes that also involve absorption and compaction. And since activation energy is inversely proportional to the reaction rate, the increasing Ea implies that there will be a progressive reduction in reaction and conversion rates at the later stages of thermal decomposition. These trends are reported in Section 3.1, where rapid decomposition is observed between 185–450 °C (2nd stage) but slow, progressive burn at later stages. The kinetic data from this study can be used in predictive and probabilistic modelling to develop realistic and efficient energy processes for HF. This can inform the design, development and optimization of complex energy systems, particularly relating to reactor sizing, design equations and performance assessment.

3.3. Evolved gas analysis

The results of the evolved gas analysis for the various feedstocks are presented in Table 3. Gas products were collected at 370 and 530 °C for HF, 350 and 435 °C for WB and 330 and 475 °C for SF corresponding to thermal stages with maximum intensities of weight loss.

3.3.1. Evolved gas products of HF at 370 and 530 °C

The results in Table 3 show that most of the chemical species from the pyrolysis of HF at 370 °C are aliphatic compounds with a high prevalence of carboxyl groups and their derivatives (acids, esters, amides etc.). The fatty acids varied from short-chain fatty acids (SCFAs) e.g. acetic acid to long-chain fatty acids (LCFAs) e.g. n-hexadecanoic acid, 9-octadecenoic acid. Several literatures have reported the abundance of SCFAs in HF, citing common examples of acetic acid, propionic acid and butyric acid (Zhao et al., 2018; Primec et al., 2017). These faecal SCFAs are produced in the colon during bacterial fermentation of undigested organic materials (Siigur et al., 1994). There are also report of LCFAs in HF (Kalivianakis et al., 2000), although relatively low in abundance, often derived from dietary plant and animal fat (Charuwat et al., 2018). In this study, long-chain fatty acids derivatives include 9-methylheptadecanoic acid methyl ester, (Z)-9-Octadecenamide, n-hexadecanamide etc. The aromatics include 4-methylphenol (p-cresol), 4-methylphenol (m-cresol), pyrrolo[1,2-a]pyridine, 4-methoxyphenol amongst others. Cresol is typically found in human excrements (urine, sweat, faeces) as a degradation product of protein (Chen et al., 2006; King et al., 2009). Pyrrolo[1,2-a]pyridine is an isomer of indole, a compound that gives faeces its characteristic odour (Brown, 1998), in addition to phenols, and skatoles (Wu and Masten, 2002; King et al., 2009). Guaiacol is a major building block in lignin formation and one of its pyrolysis products (Draelos, 2007). Jenner et al. (2005) attributed the presence of methylated aromatics in faecal water to dietary intake or metabolism of methylated polyphenols and report the inability of faecal bacteria to process polyphenols. Garner et al. (2007) consider a wide range of aromatics and nitrogen-containing derivatives of pyridine, pyrrole, and indole as a product of amino acid degradation.

At 530 °C, the decomposition products were more fragmented with higher proportions of low molecular weight alkanes and

Table 3
Evolved gas analysis of HF, WB and SF at various pyrolysis temperature.

RT	Human Faeces (HF)	370 °C	530 °C	RT	Wood Biomass (HF)	350 °C	435 °C	RT	Simulant Faeces (SF)	330 °C	475 °C
2.55	Acetic Acid	[a]	–	2.13	2-Amino-1-propanol	–	[a]	2.53	Acetic Acid	[a]	[a]
2.87	Butane	[a]	–	2.60	Acetic acid	[b]	[a]	2.86	Butane	[a]	[a]
3.04	1-heptene	–	[a]	2.85	1-hydroxy-2-propanone	–	[a]	3.03	Heptene	–	[a]
3.73	2-propenylidene-cyclobutene	–	[b]	3.85	3-amino-2-oxazolidinone	[a]	[a]	3.71	1H-pyrrole	–	[a]
3.93	2-octene	–	[a]	4.45	2-furancarboxaldehyde	[b]	[a]	3.85	Toluene	–	[a]
4.02	n-octane	–	[a]	4.68	2-furanmethanol	[b]	[b]	3.91	3-amino-2-oxazolidinone	[a]	–
4.80	1-(acetyloxy)-2-propanone	[a]	–	5.70	2-hydroxy-2-cyclopenten-1-one	–	[a]	4.44	Octene	–	[a]
4.84	Ethylbenzene	–	[b]	6.31	5-methyl-2-furancarboxaldehyde	[a]	[a]	4.67	2-furancarboxaldehyde	[a]	–
4.97	1,2-dimethylbenzene	–	[a]	6.92	2-methyliminoperhydro-1,3-oxazine	[a]	[a]	4.69	2-furanmethanol	[b]	[a]
5.20	1-nonene	–	[a]	7.28	2-hydroxy-3-methyl-2-cyclopenten-1-one	–	[a]	4.86	1-(acetyloxy)-2-propanone	[b]	[a]
5.30	n-nonane	–	[a]	8.29	2-methoxy-phenol, -/o-guaiacol	–	[a]	5.19	1-nonene	–	[a]
5.48	1-Ethylcyclopentene	–	[a]	9.49	N,N′-di-benzoyloxy-hexanediamide	–	[a]	5.26	Cyclooctatetraene	–	[a]
5.54	2-octyn-1-ol	–	[a]	9.93	2-methoxy-4-methyl-phenol/p-cresol	–	[a]	5.32	n-nonane	–	[a]
6.49	Carbamic acid, phenyl ester	[a]	[a]	10.46	5-Hydroxymethylfurfural	[a]	–	6.28	5-methyl-2-furancarboxaldehyde	[a]	–
6.73	1-decene	–	[b]	11.21	4-ethyl-2-methoxy-phenol	–	[a]	6.71	2-hydroxy-3-methyl-2-cyclopenten-1-one	–	[a]
6.87	n-decane	–	[b]	11.76	2-mthoxy-4-vinylphenol	–	[b]	7.30	3-methylphenol	–	[a]
7.26	3-methyl-1,2-cyclopentanedione	[a]	–	12.25	2,6-dimethoxy-phenol	–	[a]	8.08	1-decene	–	[b]
7.38	1-methyl-4-(1-methylethenyl)-, (S)-cyclohexene	[a]	–	13.57	3,5-dimethoxy-4-hydroxytoluene	–	[a]	8.52	1,4:3,6-dianhydro-α-d-glucopyranos	–	[a]
8.02	4-methylphenol/p-cresol	[a]	–	13.71	2-methoxy-4-(1-propenyl)-phenol	[a]	[a]	10.32	Pyrrolo[1,2-a]pyridine	–	[a]
8.04	3-methylphenol/m-cresol	–	[a]	14.11	1,6-anhydro-β-D-glucopyranose	[a]	[a]	11.56	Undecene	–	[b]
8.27	4-methoxyphenol/p-guaiacol	[b]	–	16.23	4-hydroxy-3-methoxy-benzenepropanol,	[a]	–	12.82	Hexaethylene glycol	–	[a]
8.33	(Z)-2-undecene	–	[a]	16.83	2,6-dimethoxy-4-(2-propenyl)-phenol	[a]	–	14.31	Tetraethylene glycol	[b]	–
8.46	n-undecane	–	[b]	17.20	1-(4-hydroxy-3,5-dimethoxyphenyl)-ethanone,		–	16.49	8-Heptadene	–	[b]
9.90	(Z)-3-dodecene	–	[b]	17.32	3-(4-hydroxy-3-methoxyphenyl)-2-propenal	[a]	–	17.78	Hexaethylene glycol	–	[a]
10.02	n-dodecane	–	[a]	18.14	(E)-4-(3-Hydroxyprop-1-en-1-yl)-2,6-dimethoxyphenol	[a]	–	17.88	n-Hexadecanoic acid	–	[a]
11.41	6-tridecene	–	[b]	19.99	3,5-Dimethoxy-4-hydroxycinnamaldehyde	[b]	–	19.73	Pentaethylene glycol	[b]	–
11.51	Pyrrolo[1,2-a]pyridine	[a]	–					19.78	n-hexadecanoic acid	–	[b]
11.53	Tridecane	–	[b]					19.93	Hexadecanoic acid, ethyl ester	[a]	–
12.83	Trans-9-hexadecen-1-ol	–	[a]					20.82	Hexaethylene glycol	[b]	[a]
12.94	n-tetradecane	–	[a]					21.01	Trans-13-octadecenoic acid	–	[a]
16.76	Octatriacontyl pentafluoropropionate	–	[a]					21.65	Linoleic acid ethyl ester	[b]	–
18.98	Hexadecanenitrile	[b]	[a]					21.66	Ethyl Oleate	[a]	–
19.77	n-hexadecanoic acid	[b]	–					21.79	13-octadecenoic acid	–	[b]
21.22	9-methylheptadecanoic acid methyl ester	[a]	–					21.86	9-hexadecenoic acid	–	[a]
21.54	(Z)-9-octadecenoic acid/oleic Acid	[a]	–					22.44	Octadecanoic acid, ethyl ester	[a]	–
21.77	n-octadecanoic acid/stearic acid	[a]	–					22.46	i-propyl 9-octadecanoate	–	[a]
21.95	n-hexadecanamide/palmitic amide	[a]	–					23.53	2-hydroxy-1-(Z)-9-octadecenoic acidhydroxymethyl)ethyl ester	–	[a]
23.53	(Z)-9-octadecenamide	[a]	–					23.99	Cholestan-3-ol, (3β,5β)-	[a]	–
27.31	Cholest-4-ene	–	[a]								
30.71	Cholestan-3-ol, (3β,5β)	–	[a]								

RT-Retention Time; RMF-Reverse Match Factor.
[a]RMF: 850–900.
[b]RMF: 900–999.

alkenes along with medium to long-chain fatty acids, nitriles and amines. The heavier fractions of the evolved gases are cholestanols, which are abundant in the membranes of plants, animals, and microorganisms (Dutta et al., 2007). These compounds are present in high concentrations in faecal solids (Sullivan et al., 2010) because they are eliminated from the body with other sterols via bile acid synthesis from biohydrogenation of cholesterol (Björkhem and Gustafsson, 1971). Other compounds that were present were: (a) fatty alcohols e.g. 2-octyn-1-ol, and trans-9-hexadecen-1-ol; alkenes e.g. 2-octene, 2-undecene, (Z)-6-tridecene; alkanes e.g. n-nonane, n-decane, n-dodecane. These compounds are decomposition products from carbohydrate, protein and lipids. Nitrogen-containing compounds including hexadecane nitrile are by-products of degradation of protein, organic molecules that are widely distributed in proteins of plants and animals (Kato et al., 1971), but diversity was limited in the evolved gas stream and likely lost at lower temperatures.

The evolved gas products support the multi-step decomposition characteristics described in Section 3.1 and confirm the increasing Ea. The small peak observed at about 185 °C suggest the release of extractives and other volatile organic carbons. Since Ea defines the minimum energy requirement for reaction to occur, the relatively high Ea of >200 kJ/mol observed at α of >70% shows that high energy is required to thermally dissociate the LCFAs in HF. The spectrum of organic compounds in the evolved

gas stream, that is aliphatics, fatty acids, triglycerides and sterols suggest that faecal bio-oils can have reduced oxidative stability, leading to increased volatility, acidity and viscosity. The reduced content of furan derivatives, pyran compounds and functional groups in the evolved gas products suggest limited secondary reactions for HF products. Further work will be required to examine the detailed reaction pathways and intermediates formed during the pyrolysis of HF, information that can be examined using the reaction process and intermediate product analysis tools. Insights on reaction stages and evolved gas streams can inform emission abatement options and the design of a sanitary energy conversion system for processing human faeces and for recovering value-added products or chemicals.

3.3.2. Evolved gas products of WB at 350 and 435 °C

At 350 °C, the major decomposition products from pyrolysis of WB are those associated with thermal degradation of monosaccharides and branched polysaccharides in cellulose, hemicellulose and lignin (Wang et al., 2017). Some of the pyrolysis products associated to the decomposition of carbohydrates appear in the first part of the chromatogram i.e. acetic; 2-furancarboxaldehyde; 2-furanmethanol etc. These pyrolysis stages are formed at relatively low temperatures when cleavage occurs in glycosidic bonds of cellulose molecules and low molecular weight lignin (Zhou et al., 2016; Abdelaziz et al., 2016). Demirbaş (2000) have shown that the decomposition of cellulose occurs in two stages. The first stage involves depolymerization, hydrolysis, dehydration, oxidation and decarboxylation, processes that initiate gradual decomposition and charring. The other stage prompts rapid devolatilization and formation of levoglucosan (1,6-anhydro-β-d-glucopyranose), 5-hydroxymethylfurfural (HMF) and furfural either as intermediate- or end-products (Hu et al., 2018; Chheda et al., 2007). Other pyrolysis products are alcohols, ketones, aldehydes, and phenolics, compounds that are associated with lignin degradation.

In this study, the pyrolysis products that are associated to lignin decomposition at 350 °C are hydroxyphenyls and methoxyphenols with guaiacyl or syringil structures e.g. phenol, 2-methoxy-4-methyl-(p-cresol), phenol, 2-methoxy-4-(1-propenyl)-, phenol, 2,6-dimethoxy-4-(2-propenyl)-, (E)-4-(3-Hydroxyprop-1-en-1-yl)-2,6-dimethoxyphenol, 3,5-Dimethoxy-4-hydroxycinnamaldehyde, compounds with methoxyl, hydroxyl, carboxyl and carbonyl groups and can yield various intermediate products and reaction pathways (Wang et al., 2017). The decomposition of methoxyl-groups can cause the release of smaller molecular compounds such as methane and methanol and changes to phenol-containing compounds. Other oxygenated functional groups e.g. hydroxyl, carboxyl and carbonyl groups can transform side chains and form large stable fragments. It can also cause fragmentation, leading to the release of small molecular compounds e.g. CO, CO_2 and formaldehydes. Cross-linkages can also occur between intermediate and end-products, leading to polymerization.

At higher temperatures (435 °C), pyrolysis products are similar but with higher proportions of phenolic compounds including 2-methoxy-4-methylphenol, 4-ethyl-2-methoxyphenol, 2-methoxy-4-vinylphenol, 2-methoxy-4-(1-propenylphenol. The increasing proportion of furans and phenol containing compounds in the evolved gas products indicate the tendency for polymerization of products (Demirbaş, 2000) due to secondary degradation. As the evolved gas products of WB differ to HF, by-products can be expected to differ significantly.

3.3.3. Evolved gas products of SF at 330 and 475 °C

The decomposition products from SF at 330 and 475 °C reflect initial chemical constituents: cellulose, psyllium husks, yeast, polyethylene glycol and peanut oil. Compounds such as tetraethylene, pentaethylene, hexaethylene and heptaethylene glycols are fragments of polyethylene glycol. Pyrolysis products of carbohydrate decomposition include 2-furanmethanol, 3-amino-2-oxazolidinone, 5-methyl-2-furancarboxaldehyde, 1,4:3,6-dianhydro-α-d-glucopyranose, 5-methyl-2-furancarboxaldehyde, 3-methylphenol, exhibiting some similarities to WB. Compounds such as pyrrolo[1,2-a]pyridine, 2-propanone, 1-acetyoxy-, acetic acid, butane, 1-heptene, 1-decene, cholestan-3-ol, (3β,5β)- and a number of aliphatic compounds that have similar product characteristics to HF were also present.

Long chain fatty acid ethyl esters such as hexadecanoic acid, ethyl ester, ethyl oleate and octadecanoic acid, ethyl ester were present at 330 °C. At 475°C, the gas products were more decomposed with short- to medium-chain alkanes, alkenes and aromatics (butane, toluene, 1-nonene, 1-decene, 8-heptadene etc.). Long-chain fatty acids were limited to 13-octadecanoic acid, i-propyl 9-octadecanoate, 9-hexadecenoic acid/ethyl esters. Unlike HF, where evolved gases are multiple-decomposition products of LCFAs, the pyrolysis products of SF were more of fatty alcohols. These results show that the pyrolysis of SF differs to those of HF as such, the mechanism of SF pyrolysis products cannot model those for HF accurately.

This study has provided some insights into the decomposition behaviour and products that are formed during the pyrolysis of HF and in comparison, with WB and SS. However, further work is recommended to expand the knowledge and database of decomposition of these materials, particularly for HF. Some of the limitations of this study involve sample analysis: this study has considered a sample type; however, human excreta is subject to body metabolism and gut microbiomes in individuals differ one to another. Factors such as dietary intake, fibre content, body weight, age, health conditions (Rose et al., 2015) have been shown to affect the composition of faeces; hence sample variation could yield different products.

This study has also explored electron impact (EI) ionization mode with full scan mass detection, which is most ideal for comprehensive screening of complex sample matrixes, but subject to instrumentation limits, mass discrimination effects. More so, methods rely on database searching and spectral matching with identified chemical species based on relative resemblance and not absolute. This makes it challenging for identifying unknown compounds. The selected ion monitoring mode is a more targeted approach; however, requires prior knowledge of acquisition parameters. In this regard, GC tandem quadrupole mass spectrometer (GC–MS/MS) or GC/quadrupole-time of flight (Q-TOF)/MS can further improve targeted analysis. Further analysis could also be conducted to examine the evolved gas analysis of wood biomass/human faeces blends for any synergetic effects.

4. Conclusion

This study investigated the pyrolysis behaviour of human faeces under controlled heating and atmospheric conditions. The analysis was completed using TG–GC–MS with non-isothermal, model-free approaches used for determining kinetic data. These results have been compared to wood biomass (WB) and simulant faeces (SF) to highlight key differences and similarities. Two decomposition stages are observed in the weight loss curves for pyrolysis of human faeces (HF), temperatures between 185 and 600 °C. Peak pyrolysis temperature increased from 316 to 392 °C at heat rates of 5–100 °C/min, corresponding to a maximum weight loss rate of 0.3–5.6 mg/min. The average apparent

activation energy for HF is 192 kJ/mol and best determined by KAS model. The decomposition characteristics of HF differed to WB which had a prominent decomposition peak at 415 °C and SF with multiple peaks at 315 °C, 359 °C and 455 °C. For the WB, the maximum weight loss rate was 5.86 mg/min while SF and HF were 2.90 and 3.09 g/min respectively, at the same heating rate. Blending with WB improved pyrolysis of HF, irrespective of the proportions of the blend. The evolved gas analysis shows that the decomposition products of HF are different from WB and HF. At 370 °C, pyrolysis products include 4-methoxy-phenol, n-hexadecanoic acid, phenol, 4-methyl- and indole isomer (pyrrolo[1,2-a]pyridine). At 530 °C, evolved gases were largely fragmented with high proportions of alkanes and alkenes including 3-dodecane, 2-undecane, 6-tridecene, 2-propenylidene-cyclobutene. These products differed to WB that are largely hydroxyphenyls and methoxyphenols with guaiacyl or syringil structures. Similar decomposition products with SS include pyrrolo[1,2-a]pyridine, 1-acetyoxy-2-propanone, 1-heptene, 1-decene, cholestan-3-ol, (3β,5β)- etc.; however, the evolved gas products for SS were largely high-molecular glycols and esters, including hexaethylene glycol, and octadecanoic acid, ethyl ester. Insights on reaction stages and evolved gas streams can inform emission abatement options and the design of a sanitary energy conversion system for processing human faeces and for recovering value-added products or chemicals.

CRediT authorship contribution statement

Tosin Somorin: Conceptualization, Investigation, Writing - original draft. **Alison Parker:** Resources, Funding acquisition, Supervision, Writing - review & editing. **Ewan McAdam:** Resources, Funding acquisition, Supervision, Writing - review & editing. **Leon Williams:** Resources, Funding acquisition, Supervision, Writing - review & editing. **Sean Tyrrel:** Resources, Funding acquisition, Supervision, Writing - review & editing. **Athanasios Kolios:** Resources, Funding acquisition, Supervision, Writing - review & editing. **Ying Jiang:** Resources, Funding acquisition, Supervision, Writing - review & editing.

Declaration of competing interest

The authors declare that they have no known competing financial interests or personal relationships that could have appeared to influence the work reported in this paper.

Acknowledgement

This publication is based on research funded by the Bill & Melinda Gates Foundation, USA. The findings and conclusions contained within are those of the authors and do not necessarily reflect positions or policies of the Bill & Melinda Gates Foundation.

References

Abdelaziz, O.Y., Brink, D.P., Prothmann, J., Ravi, K., Sun, M., Garcia-Hidalgo, J., Sandahl, M., Hulteberg, C.P., Turner, C., Lidén, G., Gorwa-Grauslund, M.F., 2016. Biological valorization of low molecular weight lignin. Biotechnol. Adv. 34 (8), 1318–1346.

Aboyade, A.O., Görgens, J.F., Carrier, M., Meyer, E.L., Knoetze, J.H., 2013. Thermogravimetric study of the pyrolysis characteristics and kinetics of coal blends with corn and sugarcane residues. Fuel Process. Technol. 106, 310–320.

Bai, X., Li, Z., Zhang, Y., Ni, J., Wang, X., Zhou, X., 2018. Recovery of ammonium in urine by biochar derived from faecal sludge and its application as soil conditioner. Waste Biomass Valoriz. 9 (9), 1619–1628.

Basu, P., 2010. Biomass Gasification and Pyrolysis: Practical Design and Theory. Academic press.

Björkhem, I., Gustafsson, J.Å., 1971. Mechanism of microbial transformation of cholesterol into coprostanol. Eur. J. Biochem. 21 (3), 428–432.

Brown, E.G., 1998. Indoles. In: Ring Nitrogen and Key Biomolecules. Springer, Dordrecht, pp. 192–207.

Charuwat, P., Boardman, G., Bott, C., Novak, J.T., 2018. Thermal degradation of long Chain Fatty acids. Water Environ. Res. 90 (3), 278–287.

Chen, Y.C., Higgins, M., Murthy, S., Maas, N., Covert, K., Toffey, W., 2006. Production of odorous indole, skatole, p-cresol, toluene, styrene, and ethylbenzene in biosolids. J. Residuals Sci. Technol. 3 (4), 193–202.

Chen, W.H., Kuo, P.C., 2011. Torrefaction and co-torrefaction characterization of hemicellulose, cellulose and lignin as well as torrefaction of some basic constituents in biomass. Energy 36 (2), 803–811.

Chen, D., Zhou, J., Zhang, Q., 2014. Effects of heating rate on slow pyrolysis behavior, kinetic parameters and products properties of moso bamboo. Bioresour. Technol. 169, 313–319.

Chheda, J.N., Román-Leshkov, Y., Dumesic, J.A., 2007. Production of 5-hydroxymethylfurfural and furfural by dehydration of biomass-derived mono-and poly-saccharides. Green Chem. 9 (4), 342–350.

Chun, Y.N., Kim, S.C., Yoshikawa, K., 2011. Pyrolysis gasification of dried sewage sludge in a combined screw and rotary kiln gasifier. Appl. Energy 88 (4), 1105–1112.

Danso-Boateng, E., Holdich, R.G., Shama, G., Wheatley, A.D., Sohail, M., Martin, S.J., 2013. Kinetics of faecal biomass hydrothermal carbonisation for hydrochar production. Appl. Energy 111, 351–357.

Demirbaş, A., 2000. Mechanisms of liquefaction and pyrolysis reactions of biomass. Energy Convers. Manage. 41 (6), 633–646.

Diener, S., Semiyaga, S., Niwagaba, C.B., Muspratt, A.M., Gning, J.B., Mbéguéré, M., Ennin, J.E., Zurbrugg, C., Strande, L., 2014. A value proposition: Resource recovery from faecal sludge—Can it be the driver for improved sanitation? Resources. Conserv. Recycl. 88, 32–38.

Draelos, Z.D., 2007. Skin lightening preparations and the hydroquinone controversy. Dermatol. Ther. 20 (5), 308–313.

Dutta, P.C., Przybylski, R., Eskin, M.N., 2007. Formation, analysis, and health effects of oxidized sterols in frying fat. In: Deep Frying. AOCS Press, pp. 111–164.

El Sayed, S.A., Mostafa, M.E., 2015. Kinetic parameters determination of biomass pyrolysis fuels using TGA and DTA techniques. Waste Biomass Valoriz. 6 (3), 401–415.

Farrow, T.S., Sun, C., Snape, C.E., 2013. Impact of biomass char on coal char burn-out under air and oxy-fuel conditions. Fuel 114, 128–134.

Fidalgo, B., Chilmeran, M., Somorin, T., Sowale, A., Kolios, A., Parker, A., Williams, L., Collins, M., McAdam, E.J., Tyrrel, S., 2019. Non-isothermal thermogravimetric kinetic analysis of the thermochemical conversion of human faeces. Renew. Energy 132, 1177–1184.

Garner, C.E., Smith, S., de Lacy Costello, B., White, P., Spencer, R., Probert, C.S., Ratcliffem, N.M., 2007. Volatile organic compounds from feces and their potential for diagnosis of gastrointestinal disease. FASEB J. 21 (8), 1675–1688.

Gil, M.V., Casal, D., Pevida, C., Pis, J.J., Rubiera, F., 2010. Thermal behaviour and kinetics of coal/biomass blends during co-combustion. Bioresour. Technol. 101 (14), 5601–5608.

Gold, M., Cunningham, M., Bleuler, M., Arnheiter, R., Schönborn, A., Niwagaba, C., Strande, L., 2018. Operating parameters for three resource recovery options from slow-pyrolysis of faecal sludge. J. Water Sanit. Hyg. Dev. 8 (4), 707–717.

Gvero, P.M., Papuga, S., Mujanic, I., Vaskovic, S., 2016. Pyrolysis as a key process in biomass combustion and thermochemical conversion. Therm. Sci. 20 (4), 1209–1222.

Hanak, D.P., Kolios, A.J., Onabanjo, T., Wagland, S.T., Patchigolla, K., Fidalgo, B., Manovic, V., McAdam, E., Parker, A., Williams, L., Tyrrel, S., 2016. Conceptual energy and water recovery system for self-sustained nano membrane toilet. Energy Convers. Manage. 126, 352–361.

He, W., Li, G., Kong, L., Wang, H., Huang, J., Xu, J., 2008. Application of hydrothermal reaction in resource recovery of organic wastes. Resour. Conserv. Recy. 52 (5), 691–699.

Herzen, B., Talsma, L., 2014. Conversion of Human Waste Into Biochar using Pyrolysis At a Community-Scale Facility in Kenya - Various Documents on Results from Research Grant. Stanford University and The Climate Foundation, Stanford, California, USA.

Hu, B., Lu, Q., Jiang, X., Dong, X., Cui, M., Dong, C., Yang, Y., 2018. Pyrolysis mechanism of glucose and mannose: The formation of 5-hydroxymethyl furfural and furfural. J. Energy Chem. 27 (2), 486–501.

Ieropoulos, I., Greenman, J., Melhuish, C., 2012. Urine utilisation by microbial fuel cells; energy fuel for the future. Phys. Chem. Chem. Phys. 14 (1), 94–98.

Jenner, A.M., Rafter, J., Halliwell, B., 2005. Human fecal water content of phenolics: the extent of colonic exposure to aromatic compounds. Free Radic. Biol. Med. 38 (6), 763–772.

Jurado, N., Somorin, T., Kolios, A.J., Wagland, S., Patchigolla, K., Fidalgo, B., Parker, A., McAdam, E., Williams, L., Tyrrel, S., 2018. Design and commissioning of a multi-mode prototype for thermochemical conversion of human faeces. Energy Convers. Manage. 163, 507–524.

Kalivianakis, M., Minich, D.M., Havinga, R., Kuipers, F., Stellaard, F., Vonk, R.J., Verkade, H.J., 2000. Detection of impaired intestinal absorption of long-chain fatty acids: validation studies of a novel test in a rat model of fat malabsorption. Amer. J. Clin. Nutr. 72 (1), 174–180.

Kato, S., Kurata, T., Fujimaki, M., 1971. Thermal degradation of aromatic amino acids. Agric. Biol. Chem. 35 (13), 2106–2112.
Kim, H.S., Kim, S., Kim, H.J., Yang, H.S., 2006. Thermal properties of bio-flour-filled polyolefin composites with different compatibilizing agent type and content. Thermochim. Acta 451 (1–2), 181–188.
King, R.A., May, B.L., Davies, D.A., Bird, A.R., 2009. Measurement of phenol and p-cresol in urine and feces using vacuum microdistillation and high-performance liquid chromatography. Anal. Biochem. 384 (1), 27–33.
Kolios, A., Jiang, Y., Somorin, T., Sowale, A., Anastasopoulou, A., Anthony, E.J., Fidalgo, B., Parker, A., McAdam, E., Williams, L., Collins, M., 2018. Probabilistic performance assessment of complex energy process systems–the case of a self-sustained sanitation system. Energy Convers. Manage. 163, 74–85.
Krerkkaiwan, S., Fushimi, C., Tsutsumi, A., Kuchonthara, P., 2013. Synergetic effect during co-pyrolysis/gasification of biomass and sub-bituminous coal. Fuel Process. Technol. 115, 11–18.
Kumar, G., Shobana, S., Chen, W.H., Bach, Q.V., Kim, S.H., Atabani, A.E., Chang, J.S., 2017. A review of thermochemical conversion of microalgal biomass for biofuels: chemistry and processes. Green Chem. 19 (1), 44–67.
Lens, P., Hamelers, B., Hoitink, H., Bidlingmaier, W. (Eds.), 2004. Resource Recovery and Reuse in Organic Solid Waste Management. IWA publishing.
Li, S., Chen, X., Liu, A., Wang, L., Yu, G., 2014. Study on co-pyrolysis characteristics of rice straw and shenfu bituminous coal blends in a fixed bed reactor. Bioresour. Technol. 155, 252–257.
Lin, Y., Liao, Y., Yu, Z., Fang, S., Lin, Y., Fan, Y., Peng, X., Ma, X., 2016. Co-pyrolysis kinetics of sewage sludge and oil shale thermal decomposition using TGA–FTIR analysis. Energy Convers. Manage. 118, 345–352.
Liu, X., Li, Z., Zhang, Y., Feng, R., Mahmood, I.B., 2014. Characterization of human manure-derived biochar and energy-balance analysis of slow pyrolysis process. Waste Manage. 34 (9), 1619–1626.
Lu, K.M., Lee, W.J., Chen, W.H., Lin, T.C., 2013. Thermogravimetric analysis and kinetics of co-pyrolysis of raw/torrefied wood and coal blends. Appl. Energy 105, 57–65.
Magdziarz, A., Werle, S., 2014. Analysis of the combustion and pyrolysis of dried sewage sludge by TGA and MS. Waste Manage. 34 (1), 174–179.
Mihelcic, J.R., Fry, L.M., Shaw, R., 2011. Global potential of phosphorus recovery from human urine and feces. Chemosphere 84 (6), 832–839.
Moghtaderi, B., Meesri, C., Wall, T.F., 2004. Pyrolytic characteristics of blended coal and woody biomass. Fuel 83 (6), 745–750.
Naqvi, S.R., Tariq, R., Hameed, Z., Ali, I., Naqvi, M., Chen, W.H., Ceylan, S., Rashid, H., Ahmad, J., Taqvi, S.A., Shahbaz, M., 2019. Pyrolysis of high ash sewage sludge: Kinetics and thermodynamic analysis using Coats-Redfern method. Renew. Energy 131, 854–860.
Naqvi, S.R., Tariq, R., Hameed, Z., Ali, I., Taqvi, S.A., Naqvi, M., Niazi, M.B.K., Noor, T., Farooq, W., 2018. Pyrolysis of high-ash sewage sludge: Thermo-kinetic study using TGA and artificial neural networks. Fuel 233, 529–538.
Nowicki, L., Ledakowicz, S., 2014. Comprehensive characterization of thermal decomposition of sewage sludge by TG–MS. J. Anal. Appl. Pyrol. 110, 220–228.
Nyakeri, E.M., Ogola, H.J., Ayieko, M.A., Amimo, F.A., 2017. An open system for farming black soldier fly larvae as a source of proteins for smallscale poultry and fish production. J. Insects Food Feed 3 (1), 51–56.
Onabanjo, T., Kolios, A.J., Patchigolla, K., Wagland, S.T., Fidalgo, B., Jurado, N., Hanak, D.P., Manovic, V., Parker, A., McAdam, E., Williams, L., 2016a. An experimental investigation of the combustion performance of human faeces. Fuel 184, 780–791.
Onabanjo, T., Patchigolla, K., Wagland, S.T., Fidalgo, B., Kolios, A., McAdam, E., Parker, A., Williams, L., Tyrrel, S., Cartmell, E., 2016b. Energy recovery from human faeces via gasification: a thermodynamic equilibrium modelling approach. Energy Convers. Manage. 118, 364–376.
Özsin, G., Pütün, A.E., 2017. Kinetics and evolved gas analysis for pyrolysis of food processing wastes using TGA/MS/ft-IR. Waste Manage. 64, 315–326.
Pasangulapati, V., Ramachandriya, K.D., Kumar, A., Wilkins, M.R., Jones, C.L., Huhnke, R.L., 2012. Effects of cellulose, hemicellulose and lignin on thermochemical conversion characteristics of the selected biomass. Bioresour. Technol. 114, 663–669.
Penn, R., Ward, B.J., Strande, L., Maurer, M., 2018. Review of simulant human faeces and faecal sludge for sanitation and wastewater research. Water Res. 132, 222–240.
Poletto, M., Zattera, A.J., Forte, M.M., Santana, R.M., 2012. Thermal decomposition of wood: Influence of wood components and cellulose crystallite size. Bioresour. Technol. 109, 148–153.
Primec, M., Mičetić-Turk, D., Langerholc, T., 2017. Analysis of short-chain fatty acids in human feces: a scoping review. Anal. Biochem. 526, 9–21.
Radford, J.T., Underdown, C., Velkushanova, K., Byrne, A., Smith, D.P.K., Fenner, R.A., Pietrovito, J., Whitesell, A., 2015. Faecal sludge simulants to aid the development of desludging technologies. J. Water Sanit. Hyg. Dev. 5 (3), 456–464.
Rodríguez-Abalde, Á., Gómez, X., Blanco, D., Cuetos, M.J., Fernández, B., Flotats, X., 2013. Study of thermal pre-treatment on anaerobic digestion of slaughterhouse waste by TGA-MS and FTIR spectroscopy. Waste Manage. Res. 31 (12), 1195–1202.
Rose, C., Parker, A., Jefferson, B., Cartmell, E., 2015. The characterization of feces and urine: a review of the literature to inform advanced treatment technology. Crit. Rev. Environ. Sci. Technol. 45 (17), 1827–1879.
Saldarriaga, J.F., Aguado, R., Pablos, A., Amutio, M., Olazar, M., Bilbao, J., 2015. Fast characterization of biomass fuels by thermogravimetric analysis. Fuel 140, 744–751.
Siigur, U., Norin, K.E., Allgood, G., Schlagheck, T., Midtvedt, T., 1994. Concentrations and correlations of faecal short-chain fatty acids and faecal water content in man. Microb. Ecol. Health Dis. 7 (6), 287–294.
Singh, S., Wu, C., Williams, P.T., 2012. Pyrolysis of waste materials using TGA-MS and TGA-FTIR as complementary characterisation techniques. J. Anal. Appl. Pyrol. 94, 99–107.
Slopiecka, K., Bartocci, P., Fantozzi, F., 2012. Thermogravimetric analysis and kinetic study of poplar wood pyrolysis. Appl. Energy 97, 491–497.
Somorin, T.O., Kolios, A.J., Parker, A., McAdam, E., Williams, L., Tyrrel, S., 2017. Faecal-wood biomass co-combustion and ash composition analysis. Fuel 203, 781–791.
Strande, L., Brdjanovic, D. (Eds.), 2014. Faecal Sludge Management: Systems Approach for Implementation and Operation. IWA publishing.
Sullivan, D., Brooks, P., Tindale, N., Chapman, S., Ahmed, W., 2010. Faecal sterols analysis for the identification of human faecal pollution in a non-sewered catchment. Water Sci. Technol. 61 (5), 1355–1361.
Wang, S., Dai, G., Yang, H., Luo, Z., 2017. Lignocellulosic biomass pyrolysis mechanism: a state-of-the-art review. Prog. Energy Combust. Sci. 62, 33–86.
Wang, D., Xiao, R., Zhang, H., He, G., 2010. Comparison of catalytic pyrolysis of biomass with MCM-41 and CaO catalysts by using TGA–FTIR analysis. J. Anal. Appl. Pyrol. 89 (2), 171–177.
Wang, X., Zhao, B., Yang, X., 2016. Co-pyrolysis of microalgae and sewage sludge: biocrude assessment and char yield prediction. Energy Convers. Manage. 117, 326–334.
Ward, B.J., Yacob, T.W., Montoya, L.D., 2014. Evaluation of solid fuel char briquettes from human waste. Environ. Sci. Technol. 48 (16), 9852–9858.
Wu, J.J., Masten, S.J., 2002. Oxidation kinetics of phenolic and indolic compounds by ozone: applications to simulant and real swine manure slurry. Water Res. 36 (6), 1513–1526.
Wu, Y.M., Zhao, Z.L., Li, H.B., Fang, H.E., 2009. Low temperature pyrolysis characteristics of major components of biomass. J. Fuel Chem. Technol. 37 (4), 427–432.
Xu, Q., Tang, S., Wang, J., Ko, J.H., 2018. Pyrolysis kinetics of sewage sludge and its biochar characteristics. Process Saf. Environ. Prot. 115, 49–56.
Yacob, T.W., Linden, K.G., Weimer, A.W., 2018. Pyrolysis of human feces: Gas yield analysis and kinetic modeling. Waste Manage. 79, 214–222.
Yadav, K.D., Tare, V., Ahammed, M.M., 2010. Vermicomposting of source-separated human faeces for nutrient recycling. Waste Manage. 30 (1), 50–56, 832-839.
Yuan, S., Dai, Z.H., Zhou, Z.J., Chen, X.L., Yu, G.S., Wang, F.C., 2012. Rapid co-pyrolysis of rice straw and a bituminous coal in a high-frequency furnace and gasification of the residual char. Bioresour. Technol. 109, 188–197.
Zhai, Y., Peng, W., Zeng, G., Fu, Z., Lan, Y., Chen, H., Wang, C., Fan, X., 2011. Pyrolysis characteristics and kinetics of sewage sludge for different sizes and heating rates. J. Therm. Anal. Calorim. 107 (3), 1015–1022.
Zhang, Z., Zhu, M., Zhang, D., 2018. A thermogravimetric study of the characteristics of pyrolysis of cellulose isolated from selected biomass. Appl. Energy 220, 87–93.
Zhao, L., Huang, Y., Lu, L., Yang, W., Huang, T., Lin, Z., Lin, C., Kwan, H., Wong, H.L.X., Chen, Y., Sun, S., 2018. Saturated long-chain fatty acid-producing bacteria contribute to enhanced colonic motility in rats. Microbiome 6 (1), 107.
Zhou, S., Han, L., Huang, G., Yang, Z., Peng, J., 2018. Pyrolysis characteristics and gaseous product release properties of different livestock and poultry manures: Comparative study regarding influence of inherent alkali metals. J. Anal. Appl. Pyrol. 134, 343–350.
Zhou, S., Xue, Y., Sharma, A., Bai, X., 2016. Lignin valorization through thermochemical conversion: comparison of hardwood, softwood and herbaceous lignin. ACS Sustain. Chem. Eng. 4 (12), 6608–6617.

https://dspace.org/

Pyrolysis characteristics and kinetics of human faeces, simulant faeces and wood biomass by thermogravimetry–gas chromatography–mass spectrometry methods

Somorin, Tosin; Parker, Alison; McAdam, Ewan; Williams, Leon; Tyrrel, Sean F. ...

2020-12-09
Elsevier
https://doi.org/10.1016/j.egyr.2020.11.164
Somorin T, Parker A, McAdam E, et al., (2020) Pyrolysis characteristics and kinetics of human faeces, simulant faeces and wood biomass by thermogravimetry–gas chromatography–mass spectrometry methods. Energy Reports, Volume 6, November 2020, pp.3230-3239

Downloaded from a DSpace repository. https://dspace.org/